Design and Optimization of a Nozzle
for a Needle-free Injection System

by

Gabriel Nestor Sanchez

Submitted to the Department of Mechanical Engineering in
Partial Fulfillment of the Requirements for the Degree of
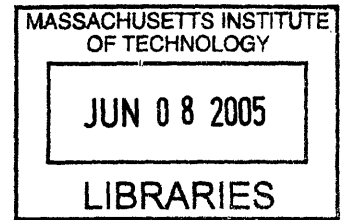
Bachelor of Science

at the

Massachusetts Institute of Technology

December 2004 [June 2005]

© 2004 Gabriel Sanchez
All rights reserved.

Signature of Author...
Department of Mechanical Engineering
December 15, 2004

Certified by...
Ian W. Hunter
Professor of Mechanical and Biological Engineering
Thesis Supervisor

Accepted by...
Ernest G. Cravalho
Professor of Mechanical Engineering
Undergraduate Officer

Design and Optimization of a Nozzle
for a Needle-free Injection System

by

Gabriel Nestor Sanchez

Submitted to the Department of Mechanical Engineering
on December 13, 2004 in Partial Fulfillment of the
Requirements for the Degree of Bachelor of Science in
Mechanical Engineering

Abstract

The purpose of this thesis was to develop an optimized nozzle for the needle-free
injection device currently under construction in MIT's Bio-Instrumentation Laboratory.
Initial predictions from ANSYS, a finite element modeling program, indicated that the
injection performance could be noticeably improved with a new nozzle design. After
running several flow simulations, a final nozzle design was selected, and a strategy was
developed to manufacture the new nozzle. The new nozzle was placed in the injection
device and measurements of the jet velocity were recorded via a high speed camera. A
2mm long nozzle with a contoured profile consisting of a linear segment tangent to an arc
segment at the nozzle exit produced an exit velocity of 45.5m/s at the end of the injection
stroke. This showed almost a 19 percent increase in velocity compared to the older
nozzle which produced 38.1m/s upon termination of the injection cycle. However, the
results of the new nozzle vary from injection to injection. Thus there is a need for
continued testing in the future, and possibly more refined measuring techniques such as
depth of penetration into the gel or developing improvements with the current video
setup.

Thesis Supervisor: Ian W. Hunter
Title: Professor of Mechanical and Biological Engineering

Acknowledgments

I would like to thank Professor Hunter and the members of MIT's Bio-Instrumentation Laboratory. In particular, I want to thank Professor Hunter for serving as my academic advisor these past four years and for granting me the opportunity to work in his Laboratory. I would also like to thank several members of the lab that helped me with the completion of this project. Andrew Taberner has served as an overall advisor and mentor throughout this process. I would like to thank him for his advice on issues related to my research. I would also like to thank Brian Hemond for providing test data for this thesis. Finally, I wish to thank to Andrea Bruno for analyzing the test data and making it more understandable.

I want to thank James McLurkin who provided a great service by proof-reading this document. In addition, would like to thank Jennifer Moore for all the hours she spent helping me proof read and format this paper.

Finally, I want to thank my family whose support throughout the years has been essential. I truly appreciate the interest they show in my education and work, and all the sacrifices they have made over the years for my benefit.

Table of Contents

1.0 Introduction

The Bio-Instrumentation Laboratory of MIT is currently developing a needle-free injection device. This thesis specifically focuses on the design and manufacturing of an optimized nozzle for the injector. Previous nozzles consisted of small holes drilled into the end of the ejection chamber. The resulting nozzle was effectively a small orifice which theoretically has a low performance. For this thesis, specific attention was given to the actual profile of the nozzle in hopes of increasing the effectiveness of the injector.

The nozzle of the injector was modeled in ANSYS, a finite element analysis program [2]. Many variations of the nozzle were created, and multiple ANSYS simulations were performed to determine the most effective shape for the profile. After comparing the results of all the nozzle variations, the best performing nozzle was selected and a manufacturing strategy was developed in order to machine the component. In order to determine the validity of the modeling program, a specific set of verification experiments were performed and the results were compared to a table of experimentally determined values.

A prototype of the nozzle was created and attached to the device testing apparatus under development by Brian Hemond of the Bio-Instrumentation laboratory. Data were collected that demonstrated an improvement in performance thanks to the nozzle redesign. However, more testing will be required in the future to determine the exact characteristics of the new nozzle, and the extent of improvement.

2.0 Background

One of the design requirements for the needle-free injector is that it be capable of the rapid delivery of multiple doses. In a portable device, each shot draws power from the batteries, and it is important to make the drug delivery process as efficient as possible. In particular, the nozzle serves as a potential region for significant energy loss. Some experimental data demonstrates that when different nozzles are subjected to the same pressure change, they will have different exit velocities. Because the penetration, and thus the effectiveness, of the needle-free injector has a significant dependence on the exit velocity of the fluid, both the performance of the device and its battery life can be improved by developing a more efficient nozzle.

2.1 Bernoulli Approximation

Bernoulli's equation can be applied to the nozzle of the device in order to develop an approximation for the nozzle performance. Because Bernoulli's equation relates only to non viscous flows, this calculation serves as an upper limit on the performance of any nozzle. First, consider a pipe with different inlet and outlet diameters subject to a change in pressure along its length. Conservation of mass requires that the mass flow rate of the inlet be equal to that of the outlet. This results in the expression shown in Equation (1):

$$Q = \frac{\pi}{4} D_{in}^{2} V_{in} = \frac{\pi}{4} D_{out}^{2} V_{out} , \tag{1}$$

where Q is the mass flow rate through the pipe, D_{in} and V_{in} are the diameter and average velocity of the pipe at the inlet, and D_{out} and V_{out} are the diameter and average velocity of the pipe at the outlet. Application of Bernoulli's equation to the pipe yields the relationship in Equation (2):

$$P_{in} + \frac{1}{2} \rho V_{in}^{2} = P_{out} + \frac{1}{2} \rho V_{out}^{2} , \tag{2}$$

where P_{in} is the pressure applied across the inlet, and P_{out} is the pressure applied at the outlet. The combination of Equations (1) and (2) leads to the relationship shown in Equation (3):

$$V_{out,B} = \left[\frac{2(P_{in} - P_{out})}{\rho(1 - (D_{out}/D_{in})^{4})} \right]^{1/2} , \tag{3}$$

Where $V_{out,B}$ represents the Bernoulli approximation of the exit velocity. Thus Equation (3) represents the maximum exit velocity for an applied pressure for the needle-free device.

2.2 Consideration of Viscous Losses

While the relationship in Equation (3) is useful for determining the maximum exit velocity, experimental data must be used to make predictions of the exit velocity that is possible when viscous losses are present. By setting D_{out}/D_{in} equal to β, and applying a scaling factor called the discharge coefficient, C_d, to account for viscous losses, the following expression is attained:

$$V_{out} = C_d \left[\frac{2(P_{in} - P_{out})}{\rho(1-(\beta)^4)} \right]^{1/2} = C_d \cdot V_{out,B} \,, \tag{4}$$

Dimensional analysis for the nozzle design suggests that C_d is a function of the Reynold's number and the ratio β. Experimental data for three different nozzle types describes the dependence of C_d on these two factors.

In effect the drag coefficient indicates how close to the Bernoulli approximation a given nozzle performs. Experiments have been conducted on the orifice, long radius, and Venturi type nozzles, shown in Figures (1), (2) and (3) below [1].
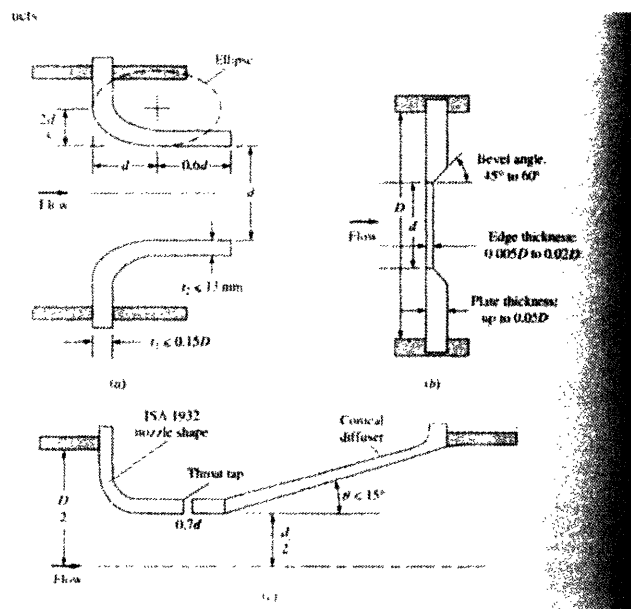

Figure 1: Description of three measured nozzle types. (Taken From White pg. 420)
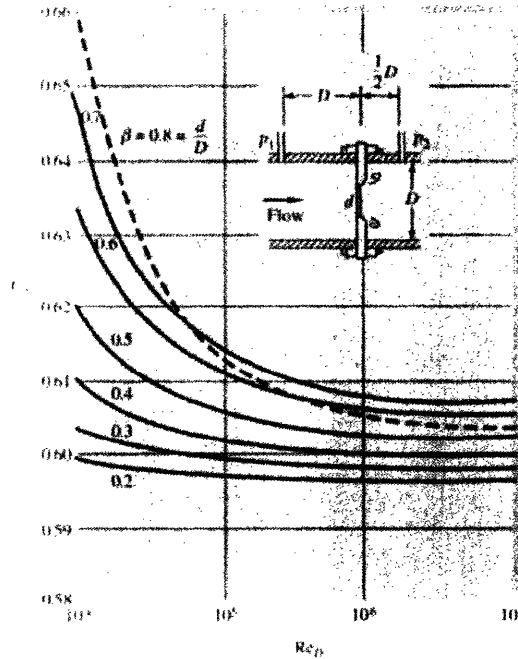
7

Figure 2: Discharge coefficient for orifice type nozzles. (Taken From White pg. 420)
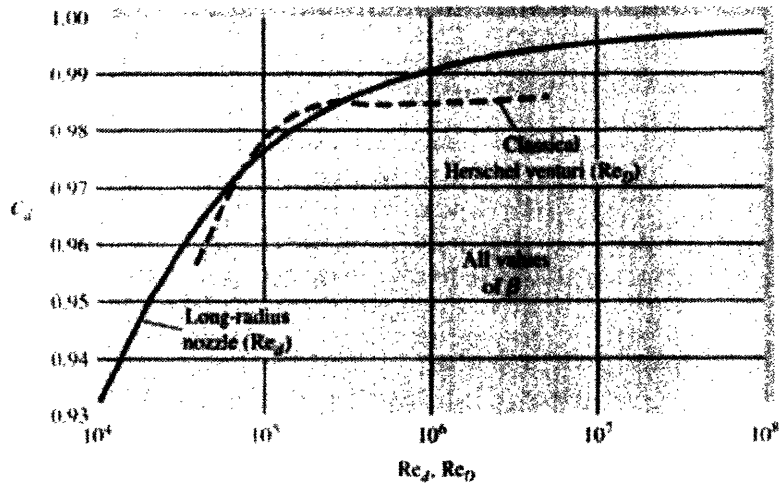

Figure 3: Discharge coefficients for the Long-radius and Herschel venture type nozzles. (Taken From White pg. 420)

The results show that the orifice has the worst discharge performance for a given pressure. As Figure (2) indicates, the exit velocity for an orifice ranges from about 60 to 70 percent of the

8

Bernoulli approximation depending on the Reynolds number and value of β. The long radius nozzle and the Venturi nozzles on the other hand have discharge coefficients near unity as can be seen in Figure (3).

In the past, the needle-free injector utilized a nozzle that was effectively an orifice. Based on the data shown in Figure (2), this is not a favorable solution. The curve shown in Figure (3) indicates that machining a nozzle with a rounded profile would bring the exit velocity to around 90% of the Bernoulli prediction. This means that for the same energy requirement as the older model, the ability of the injector to penetrate the skin would be greatly improved.

3.0 Nozzle Design

The process of re-designing the nozzle involved several steps. First, specifications were developed to determine what performance criteria a successful nozzle needed to satisfy. Two factors were used to measure the effectiveness of a given nozzle. The first was the comparison between the measured exit velocity and the Bernoulli predicted exit velocity which was referred to in Section 2.0 as C_d. The second was the vector component of the velocity in the direction perpendicular to the direction of flow. Desirable nozzles would produce a flow that was almost entirely parallel to the direction of the axis. This would prevent the jet from spreading and will minimize the size of the drug entry point on the skin. Having defined these specifications, several variations of the nozzle were tested using ANSYS, a finite element analysis program that can solve fluid flows. Finally a manufacturing technique was developed in order to produce and test the most promising nozzle based on the ANSYS solutions.

3.1 Finite Element Simulations

There were two key components to the finite element model. The first was the mesh, the finite element description of the nozzle geometry. The second component consists of the applied boundary conditions. Because many nozzles were to be tested and compared, a consistent set of boundary conditions was used for all tests. The effectiveness of each nozzle was determined by measuring the discharge coefficient and observing the shape of the jet as it left the nozzle. In addition, the current orifice nozzle was modeled to estimate how much improvement could be expected.

3.1.1 The Applied Boundary Conditions

Previous research has demonstrated that a jet traveling at approximately 100 m/s through an exit diameter of about 100μm can penetrate the skin to a depth of several millimeters [4], [7]. As Equation (3) indicates, for a given fluid the Bernoulli prediction for the exit velocity is dependent only on the ratio β, and the applied pressure difference. In the previous injector device, the inlet diameter was 3 mm at the piston cylinder, and the outlet diameter at the nozzle was 100μm. The resulting value of β was calculated to be:

$$\beta = 0.0333.$$

Using this value of β, Equation (3) thus reduced to:

$$V_{out} = 1.000000617 * \left[\frac{2(P_{in} - P_{out})}{\rho} \right]^{1/2} \approx \left[\frac{2(P_{in} - P_{out})}{\rho} \right]^{1/2}.$$

The drug in the injector was modeled as water having a density of $998\,kg/m^3$ and viscosity of $1 \times 10^{-3}\,Ns/m^2$.

For meaningful comparisons, all tests modeled the drug as water and subjected the flow to change in pressure of 5 MPa. This resulted in a Bernoulli approximation for the velocity of 100.1002 m/s or approximately 100 m/s. Equation (4) implies that C_d is the ratio of the measured outlet velocity divided by the Bernoulli approximation for the outlet velocity. However since the Bernoulli velocity is approximately 100 m/s, the ANSYS solution represents the value of $C_d \cdot 100$ for the applied pressure. Thus the value of C_d for each nozzle type was easily determined by measuring the average exit velocity from the ANSYS analysis and dividing by 100.

Dynamic boundary conditions were also required for each test. All nodes in contact with the nozzle were constrained in all directions to represent the no-slip wall condition. In addition, all nodes at the inlet had constrained velocities in the x direction to simulate the no-slip interaction with the piston surface. The nodes in contact with the piston were prescribed a pressure of 5 MPa. At the outlet, the nodes were unconstrained with respect to velocity, and were given a constant pressure of 0 MPa. Finally, all nodes lying on the axis of symmetry were constrained to move only in the y direction.

In ANSYS it is important to distinguish what type of flow is expected. The Reynolds number for the fluid flow at the exit of the nozzle can be calculated using the relation ship shown in Equation (5):

$$\text{Re}_d = \frac{\rho V D}{\mu}. \tag{5}$$

Where Re_d represents the Reynolds number at the nozzle exit, ρ is the density of the fluid, D is the diameter of the nozzle at the exit, and μ is the viscosity of the fluid. Modeling the drug as water, the value of Equation (5) becomes:

$$\text{Re}_d = \frac{998 * 100 * 100E - 6}{1.0E - 3} = 9,980.$$

Since values of Re_d around 10,000 are generally considered fully turbulent, ANSYS' turbulent solver was needed to accurately model the dynamics of the nozzles [5].

11

3.1.2 Drawing the Mesh

ANSYS has the ability to import a solid model directly into its database. Several nozzles of various profiles were constructed in SOLID EDGE [3], and imported into ANSYS for meshing. The profiles tested were the arc tangent to a line, linear, arc, parabolic, hyperbolic, and orifice profiles. Profiles were chosen and modified in order to iteratively determine the nozzle with the greatest discharge coefficient. Each profile type was drawn for various nozzle lengths. This was accomplished by using the same type of curve to connect the inlet and outlet diameters. For example, the set of "arc" profiles all use an arc to make the cross section of a nozzle with the same inlet and outlet diameters, although the distance between the inlet and outlet varies with the radius of the arc.

All of the profiles were drawn such that the slope of the profile was parallel to the axis of the nozzle at the exit with the exception of the linear profile. It was believed that this would result in a narrower, more controlled jet stream at the exit, which would make the area of penetration smaller. The "arc tangent to a line" profile contains a small arc drawn tangent to the nozzle exit, and tangent to a line that extends to the large diameter of the inlet. The only unconstrained dimension in this profile was the radius of the fillet. Nozzles of lengths 2 mm, 4 mm, 6 mm, and 8 mm were tested in ANSYS. A cross section the "arc tangent to a line" nozzle can be seen in Figure (4) with units given in millimeters.
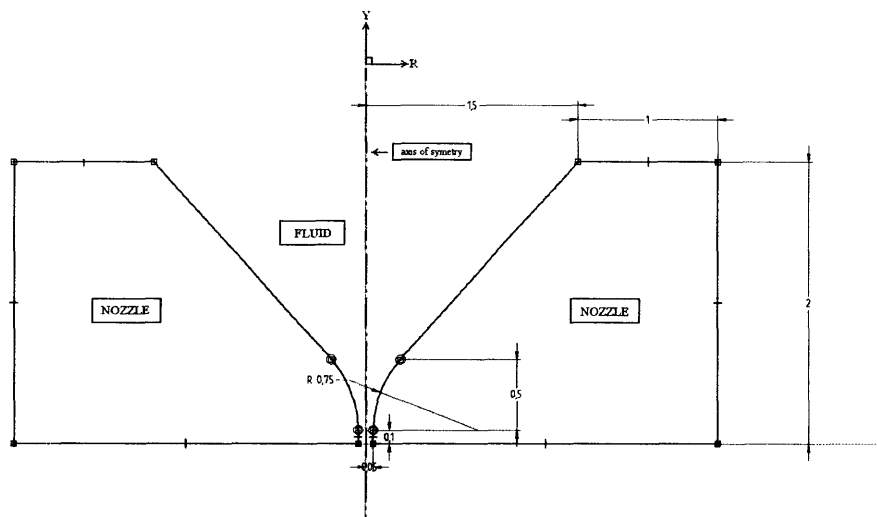

Figure 4: "arc tangent to a line" profile.

12

The linear profile was the simplest nozzle profile other than the orifice. A line connects the large diameter of the inlet cylinder to the small diameter at the exit of the nozzle. The only variable for this nozzle was the angle between the line of the nozzle surface and the axis of the nozzle. Since the outlet and inlet diameters are fixed, this is a function of the overall nozzle length. The line was then revolved around the y-axis to produce the internal surface of the nozzle. Nozzles of lengths 2 mm, 4 mm, 6 mm, and 8 mm were tested in ANSYS. An example of the linear profile nozzle can be seen below in Figure (5).
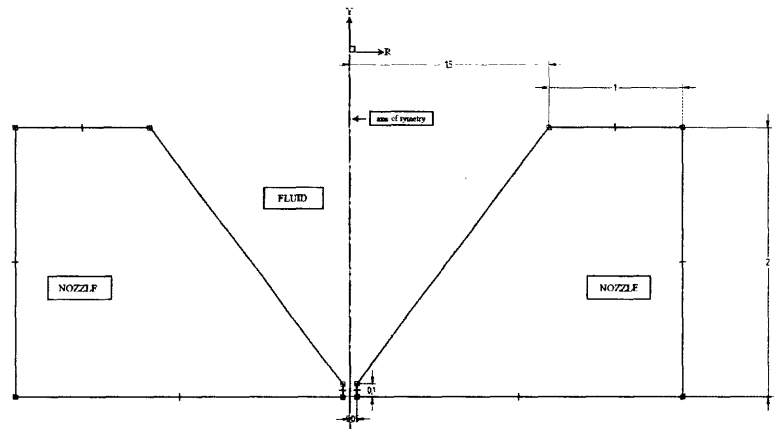

Figure 5: linear profile

The arc profile was similar to the "arc tangent to a line" profile, however the line was removed and the arc extended all the way to the large diameter of the inlet. Nozzles of lengths 2 mm, 4 mm, 6 mm, and 8 mm were tested in ANSYS. An example of the arc profile can be seen below in Figure (6).
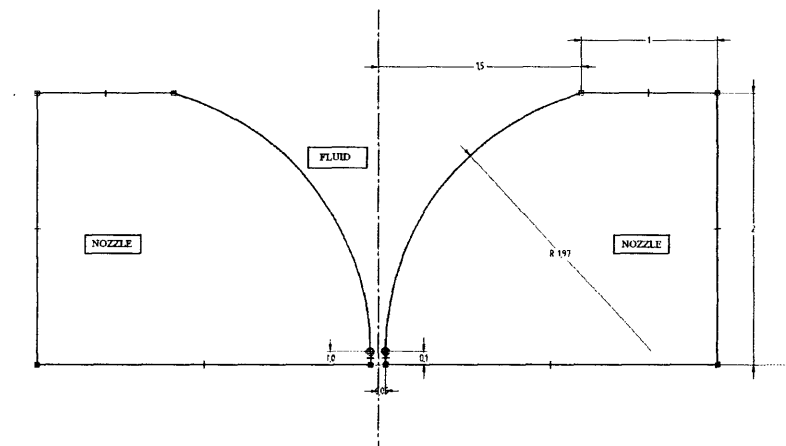

Figure 6: arc profile

13

The parabolic profile consisted of a parabola with its vertex at the nozzle exit. The parabola opened in the positive R direction so that its slope was vertical at the nozzle exit. The parabola was drawn by deriving the equation for the curve, then placing corresponding points in the solid model. A continuous curve connected the points, approximating the overall shape of the parabola. Nozzles of lengths 2 mm, 4 mm, 6 mm, and 8 mm were tested in ANSYS. An example of the parabolic profile can be seen below in Figure (7).
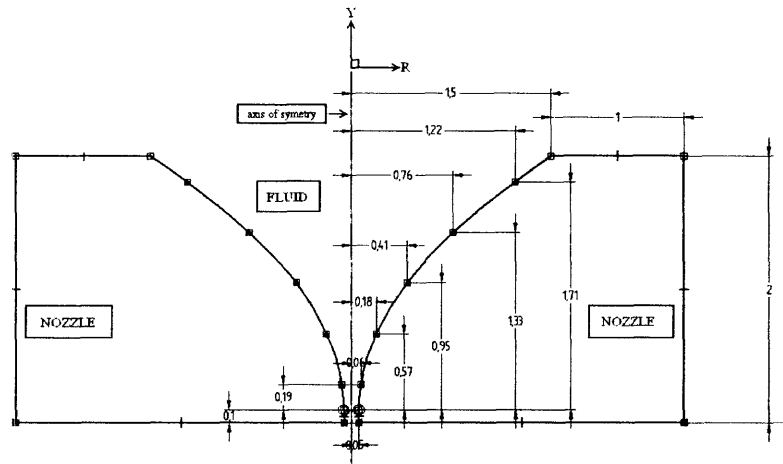

Figure 7: parabolic profile.

The hyperbolic profile was drawn in the same manner as the parabolic profile. The vertex of the parabola was placed at the nozzle exit and it opened in the positive R direction so that its slope was vertical at the nozzle exit. Nozzles of lengths 2mm, 4mm, 6mm, and 8mm were tested in ANSYS. An example of the hyperbolic profile can be seen below in Figure (8).
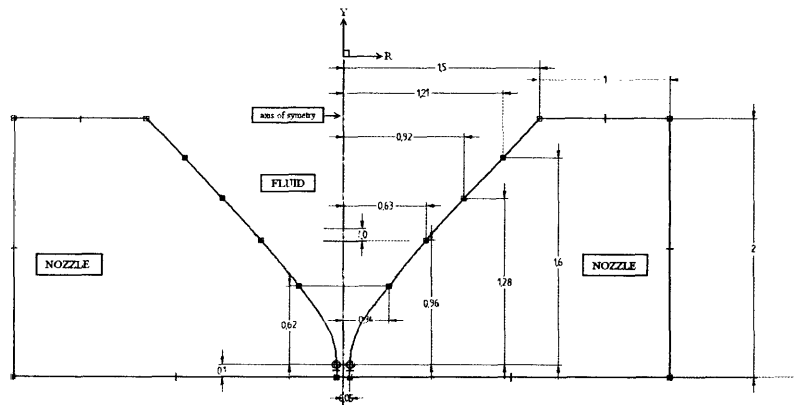

Figure 8: hyperbolic profile.

Finally, the orifice profile was modeled based on the nozzle used previously in the injection device. It consists simply of a small hole drilled in the end of a cylinder. An example of the orifice profile and its mesh can be seen below in Figure (9).
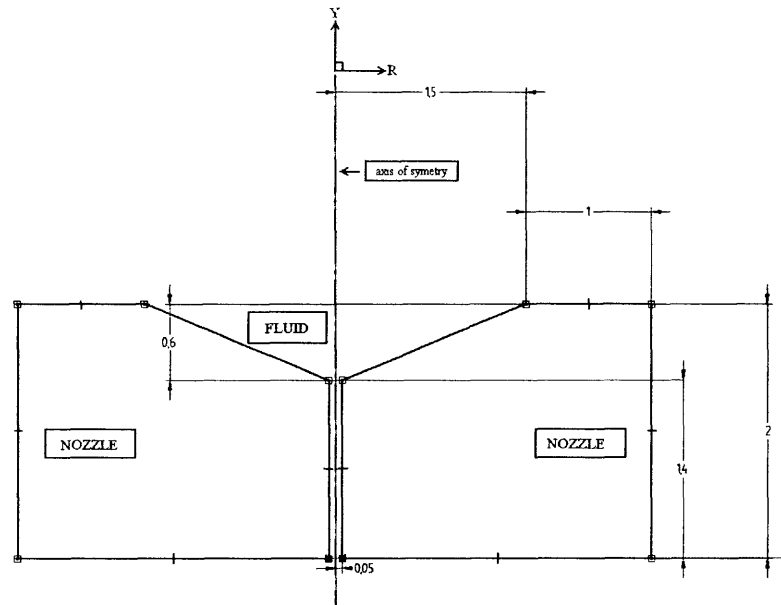

Figure 9: orifice profile.

The nozzle was modeled as a rigid body that remains in contact with the flowing fluid. The mesh was drawn as a section cut from a nozzle whose axis is collinear with the positive y-axis. First the nozzle is intersected by the XY plane through the axis creating a cross section similar to the image in Figure (4). The nozzle is then intersected by the YZ plane through the axis again, leaving only one side of the planar cross section of the nozzle. An example of the mesh for the "arc tangent to a line mesh" is shown below in Figure (10).
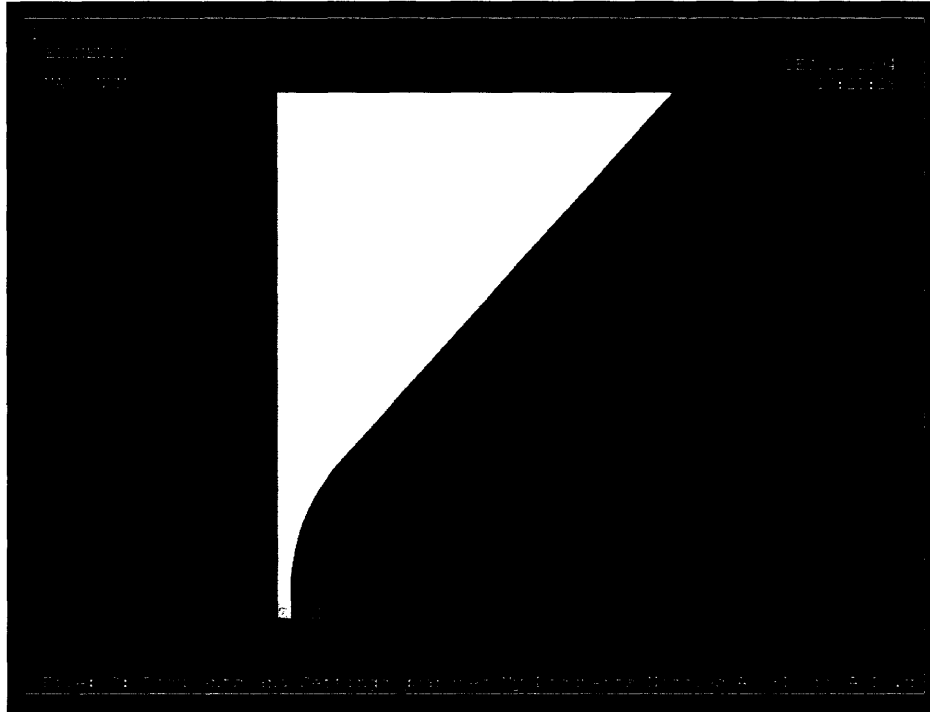
Figure 10: "arc tangent to a line" mesh in ANSYS.

ANSYS is capable of solving the 2D flow as an axi-symetric problem. Thus the two dimensional problem was defined and ANSYS produced results for the revolved cross section of the nozzle about the positive y-axis.

3.1.3 Analyzing the Results

The values of interest in these tests were the vector components of the velocity at the nozzle exit, and the magnitude of the average velocity at the nozzle exit. The vector components were easy to check because ANSYS could return the vector velocity of all nodes at the nozzle exit. Better performing nozzles would have smaller components of the exit velocity in the R direction with respect to the mesh as shown in Figure (5). There was not a specific requirement for how small the R direction component of the nozzle had to be. Nozzles were simply compared relative to each other to determine which had the least amount of spreading.

16

The average velocity at the nozzle exit can be defined as the net fluid flux through the circular region defined by the exit diameter of the nozzle. To determine the average value of the exit velocity, Equation (6) was used.

$$V_{Ay} = \frac{\iint_A V_y(r) * dA}{A_{NE}} \;,$$ (6)

where V_{Ay} is the average velocity in the y direction, $V_y(r)$ is the velocity in the y direction at some radial coordinate, r is the radial coordinate of the node, and A_{NE} is the cross sectional area of the nozzle at the exit . Only the y component was considered because this is the component parallel to the axis of symmetry and thus is the only contribution to the flux. Equation (6) can be reduced by substituting in the value of A_{NE} and realizing that $V_y(r)$ is a function of r only. Using cylindrical coordinates, Equation (6) reduces to the form:

$$V_{Ay} = \frac{\int_0^{D_{out}/2} \int_0^{2\pi} V_y(r) * r * dr d\theta}{\pi D_{out}^2/4} = \frac{2\pi \int_0^{D_{out}/2} V_y(r) * r * dr}{\pi D_{out}^2/4} \;,$$

finally resulting in Equation (7) shown below:

$$V_{Ay} = \frac{2 \int_0^{D_{out}/2} V_y(r) * r * dr}{D_{out}^2} \;.$$ (7)

To determine the average exit velocity, the results from the ANSYS analysis for several nodes along the nozzle exit were obtained and pasted into a spreadsheet. Results were developed for each profile type, as well as the various lengths of each profile type. The product of $V_y(r)$ and r was plotted against r and the area under the curve was approximated by utilizing the trapezoidal rule. The resulting value was then multiplied by the fraction $2/D_{out}^2$ to determine the value of the expression in Equation (7). Finally, the nozzle's discharge coefficient was calculated by dividing V_{Ay} by 100.

3.1.4 Verification Tests

To determine the validity of the finite element predictions, several verification tests were completed. Figures (2) and (3) display the discharge coefficients of several nozzle types. The long radius nozzle, as shown in Figure (1) was chosen for the verification tests because it has the

17

most similar nozzle properties to the proposed nozzles for the injector. The nozzle was modeled

as described in White [1] and an ANSYS simulation was performed. An example of the long-

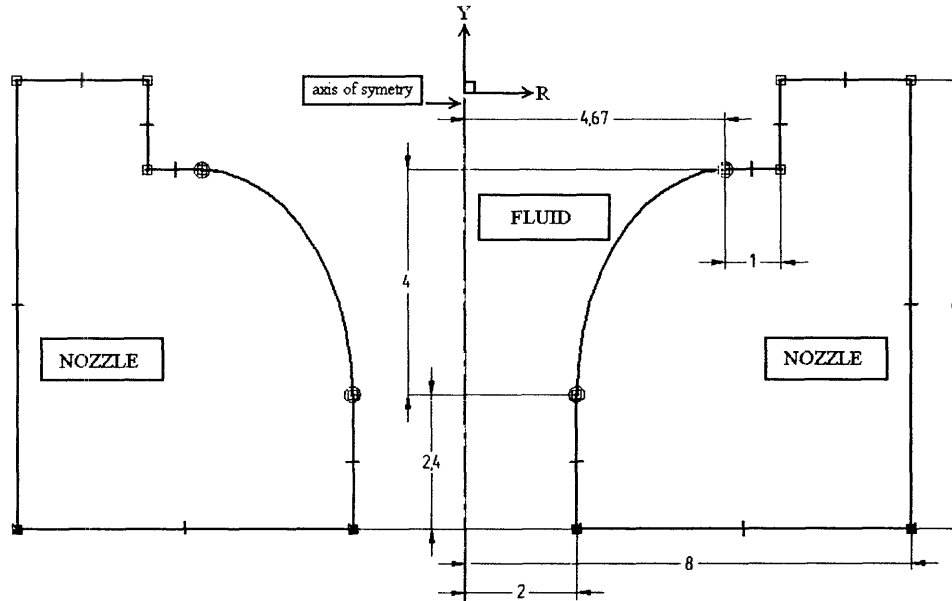radius nozzle profile can be seen below in Figure (11).

Figure 11: long-radius profile.

The discharge coefficient for the long radius nozzle can be modeled as a function of Re_d only,

which is the Reynolds number at the nozzle exit. The simulation was run several times with

varying magnitudes of applied pressure. The discharge coefficient was plotted against the $\log_{10}$

of the Re_d, and the curve was compared to the data in White [1]. The comparison demonstrated

how accurately the ANSYS code was modeling the long radius nozzle, and gave an indication of

how accurately it was modeling the nozzles for the needle-free injector.

3.2 Manufacturing the Nozzle

After reviewing the results from the ANSYS simulations a strategy was developed to

manufacture the most successful nozzle shape based on the ANSYS predictions. After

considering several options, it was decided that a custom set of drills would be produced which

could drill out the desired profile.

Most drill bits have some sort of angle at the cutting surface. However purchased bits

cannot be easily altered to drill out a specific profile. It was discovered that the Wire EDM

machine could be used to manufacture a drill bit where the cutting surface matched the cross

18

section of the desired profile. This could then be fed into a material, leaving a hole in the shape of the desired profile.

A piece of drill rod was placed in the Wire EDM and the nozzle profile was cut out with its width at any point down the nozzle scaled down by a factor of $\sqrt{2}$. This is due to the fact that when the bit spins, the profile is defined by the diagonal of the square that remains. The chuck was rotated 90 degrees and the profile was cut again. The result was a shape that had the desired profile defined by the diagonals of the bit. It looks like an extruded square of varying dimension that produces the profile. A test bit was created to drill out a nozzle with an exit diameter of 0.75 mm. The profile was an arc, and the nozzle was made out of PMMA so that the shape could be seen through the plastic. A picture of the completed test bit is shown in Figure (12), and a picture of the nozzle in the plastic is shown in Figure (13).
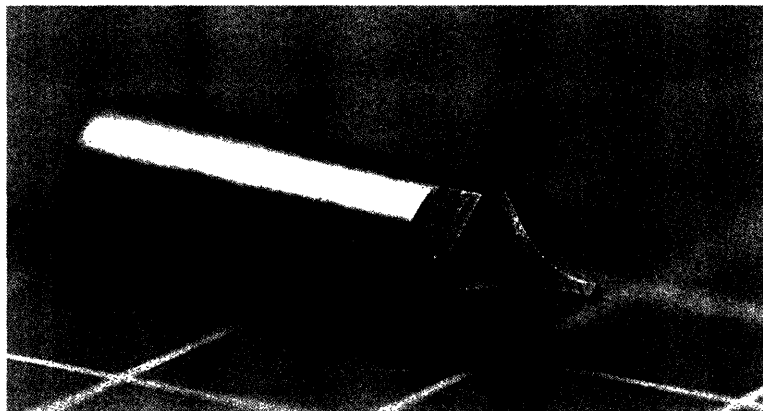

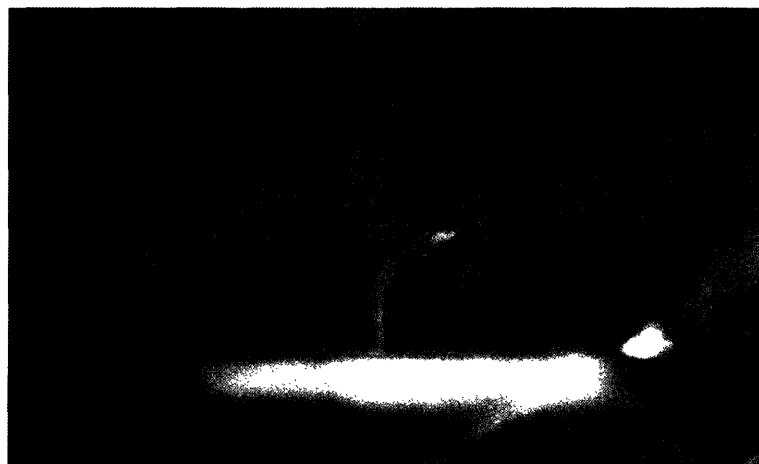Figure 12: Test Bit manufactured with the Wire EDM Machine.

Figure 13: Test nozzle drilled out of PMMA with the test bit.

19

As Figure (13) indicates, the method of producing a custom drill bit worked well for making the test nozzle. Thus the same procedure was used to manufacture bits to make the nozzles for the injector. 3 mm stainless steal precision drill rod was cut on the wire EDM to produce a bit with an exit diameter of 100 μm. An image of the completed bit under magnification is shown in Figure (14).

Figure 14: Magnified view of a completed nozzle drill bit.

When the bit was completed, a 32 mm diameter delrin wafer was machined to have a 6-hole bolt pattern which could attach to Brian Hemond's injection apparatus, and was milled down to a thickness of 2 mm. Next a 100 μm drill bit and the micro mill were used to pre-drill a hole through the 2 mm wafer. Finally the custom bit was placed in the micro mill and fed into the pre-drilled hole. This process was performed slowly and with plenty of coolant leaving a hole that had the desired contour. The wafer was then bolted to the testing apparatus and tested to determine the performance of the nozzle. A picture of the completed nozzle and the bit used to create it are shown in Figure (15).
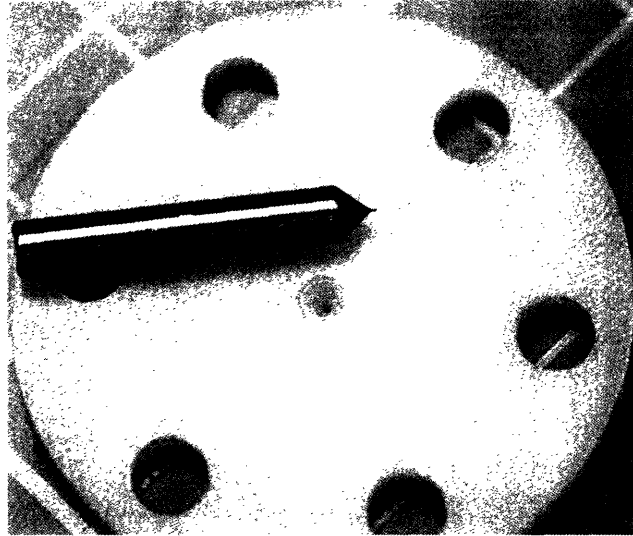
Figure 15: Completed nozzle and custom bit used to create it.

3.3 Measuring Nozzle Performance

The velocity of the jet exiting the nozzle was the primary indication of the success or failure of the nozzle. The closer the actual velocity of the jet was to the Bernoulli approximation, the higher the discharge coefficient and the better the nozzle. The nozzle was attached to the injecting and a peak pressure and 30 MPa was applied. First the new nozzle was tested several times. The new nozzle was then removed and the old nozzle was put in its place. This reduced the likelihood of the injector parameters changing between tests. An image of the testing apparatus developed by Brian Hemond is shown below in Figure (16).
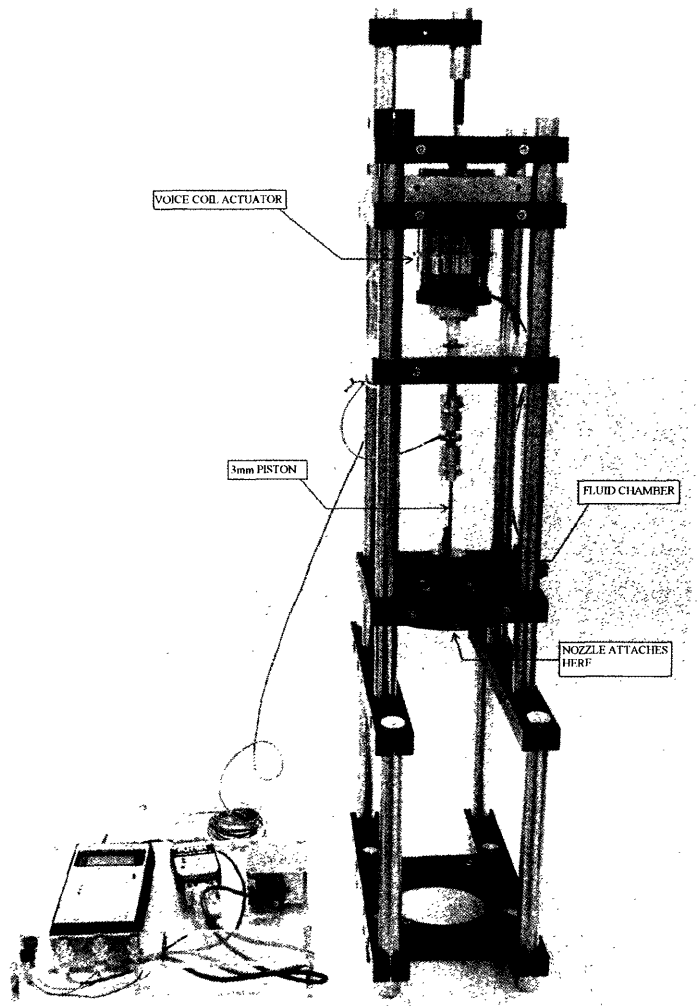
Figure 16: Testing apparatus.

A high speed video camera was used to record the water jet as it was ejected from the new nozzle. The flow was recorded at a frame rate of 71 μs per exposure with a resolution of 66.6 pixels/mm. After the video had been captured, a ruler was placed in the background to give an indication of scale. The video frames were then analyzed to produce a plot of the velocity of the jet vs. time leaving the injector.

The other measure of performance was the extent of spreading of the water jet as it left the nozzle. Since there was no quantitative value to compare, the video stills were placed side by side and a visual comparison was made by determining how much deviation had occurred from the nozzle axis at a given distance from the nozzle exit.

4.0 Results

The results of this thesis comprise the finite element analysis results (which aided in determining the optimum profile) and the measured data taken from the test apparatus. After the ANSYS predictions were analyzed, a completed nozzle was successfully manufactured and tested with the injecting mechanism. The measured results for the new nozzle were compared to the ANSYS predictions, and to the results of the previous nozzle.

4.1 Finite Element Results

The following sections will describe the results calculated with the ANSYS simulation.

4.1.1 Nozzle Discharge Coefficients

The dynamic solution for the fluid flow through the nozzle was solved using ANSYS. The nodal results from ANSYS were pasted into a spreadsheet and the average exit velocity for each shape and length was determined by approximating the area under the $V_y(r) \cdot r$. The function $V_y(r)$ is the velocity of the exiting fluid in the direction of the nozzle axis at some radial coordinate r from the axis. For each nozzle shape, the average velocity was determined for nozzle lengths of 2 mm, 4 mm, 6 mm, and 8 mm. The results were plotted for ease of comparison. Examples of these plots are shown below in Figures (17) and (18) for the nozzle with an "arc tangent to a line" as its profile. Figure (17) shows a plot of the velocity of the jet at some r vs. its radial coordinate. Figure (18) is a plot of the velocity multiplied by its radial coordinate. The area under the graph in Figure (18) gives the weighted average velocity of the jet.
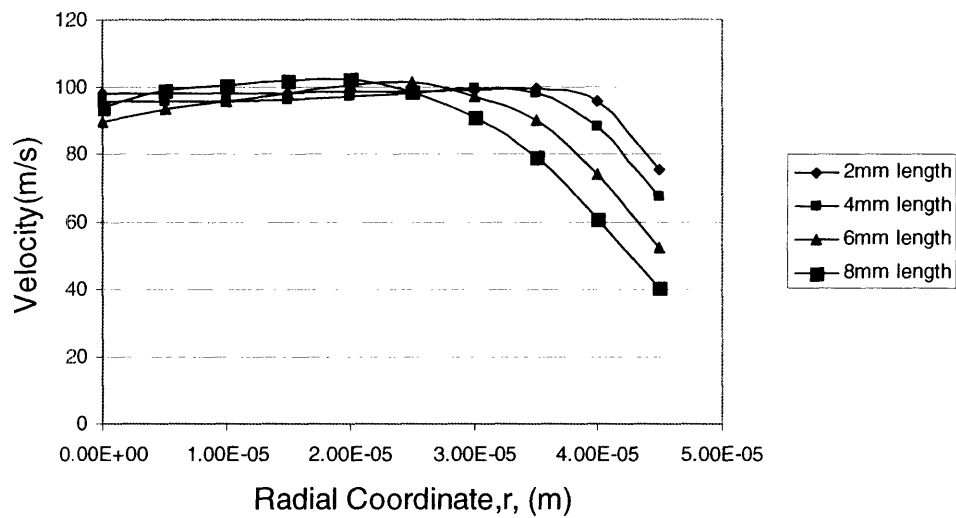
Figure 17: Velocity versus Radial Coordinate for "arc tangent to a line" profile.
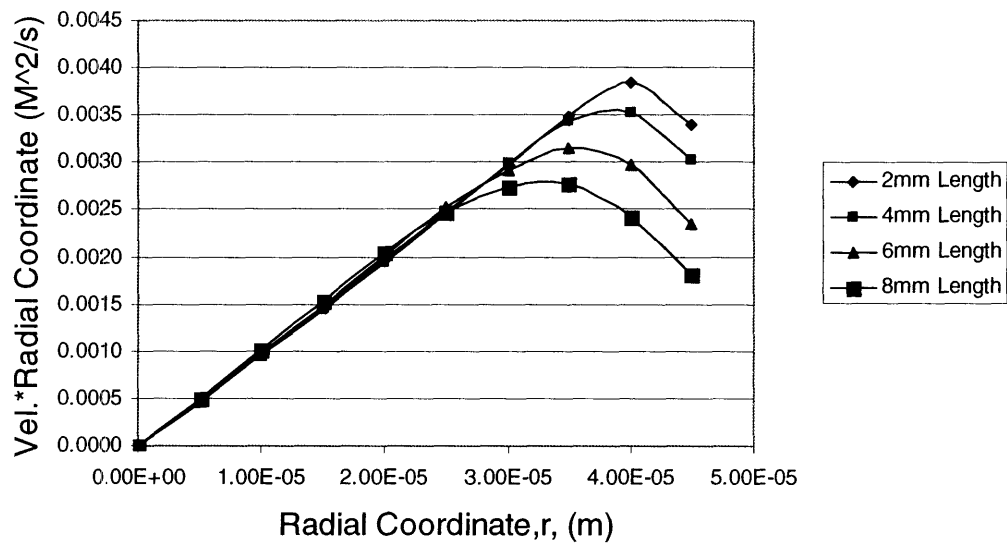

Figure 18: $V_y(r) \cdot r$ versus Radial Coordinate for "arc tangent to a line" profile.

The area under the plot in Figure (18) was estimated using the trapezoidal rule. The average velocity was then calculated using the relationship discussed in Equation (7). This velocity was divided by the Bernoulli approximation to determine the discharge coefficient for each of the nozzle types and lengths. Figure (19) shows the dependence of C_d on the nozzle length and shape for the "arc tangent to a line" profile.
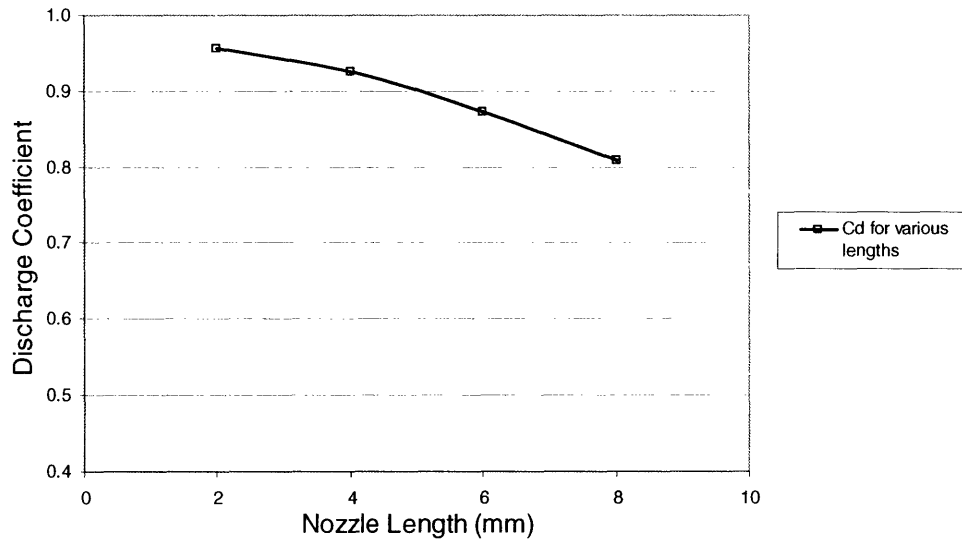
Figure 19: Discharge Coefficient versus Nozzle Length for the "arc tangent to a line" profile.

Similar plots were made for each nozzle type so that a direct comparison of performance could be conducted. Figure (20) displays the discharge coefficient plots for all nozzle types over the length range of 2mm to 8mm.
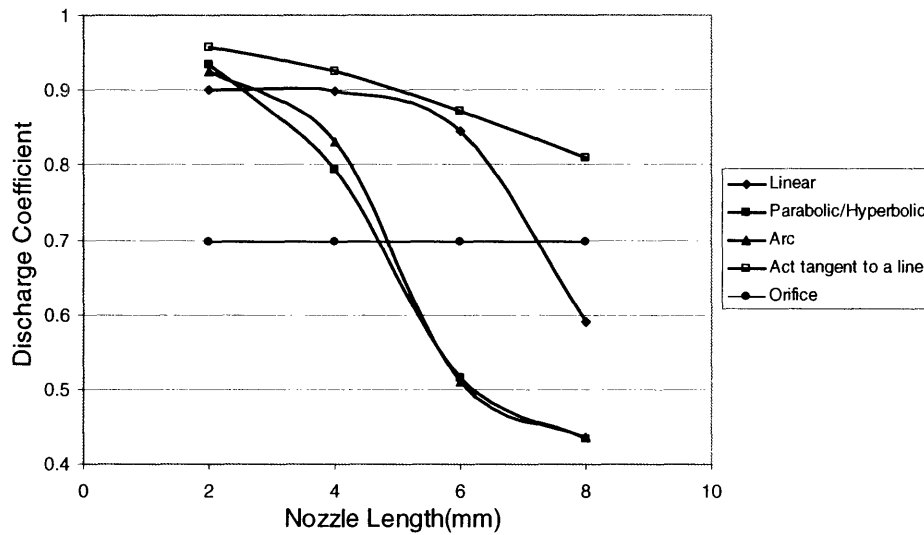

Figure 20: Discharge Coefficient versus Nozzle Length for all profiles

The Table in the Appendix B, contains the specific numerical values that are graphically represented in Figure (20).

4.1.2 Verification Results

A set of verification tests were run to quantify the validity of the ANSYS solutions. A long radius nozzle as described in White [1] was solid modeled and ANSYS was used to predict the nozzle's discharge coefficient as a function of Re_d, which is the Reynolds number at the nozzle exit. The data acquired from the ANSYS predictions was compared to the data in White [1]. Figure (21) shows a plot of the ANSYS solutions and the data from Figure (3) at various values of Re_d.
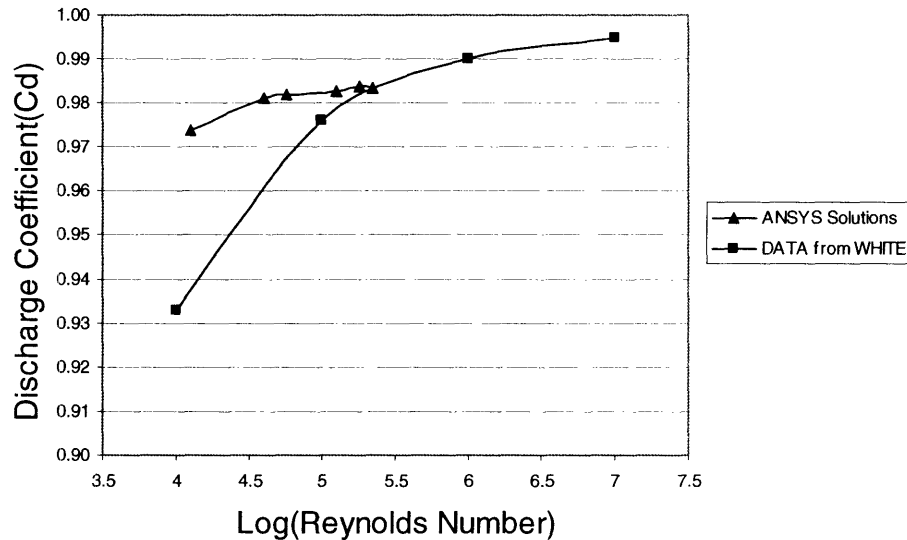
Figure 21: C_d versus Re_d for a long radius nozzle.

This graph indicates that the ANSYS prediction is within 5 percent error at a Reynolds number of 10^4, and has close to zero error at a Reynolds number of about $10^{5.5}$.

4.1 Experimental Results

The manufactured nozzles were attached to the injection device shown in Figure (16) and its performance was measured against the previous orifice nozzle. Based on the ANSYS predictions, the nozzle design with the highest discharge coefficient was the "arc tangent to a line" profile as can be seen in Figure (20). Thus a version of this nozzle was produced as

described in Section 3.2 of this thesis. The high speed video camera utilized in Brian Hemond's testing apparatus was used to record a water jet ejected from the new nozzle. Images of the jet leaving the new nozzle are shown below in Figure (22).
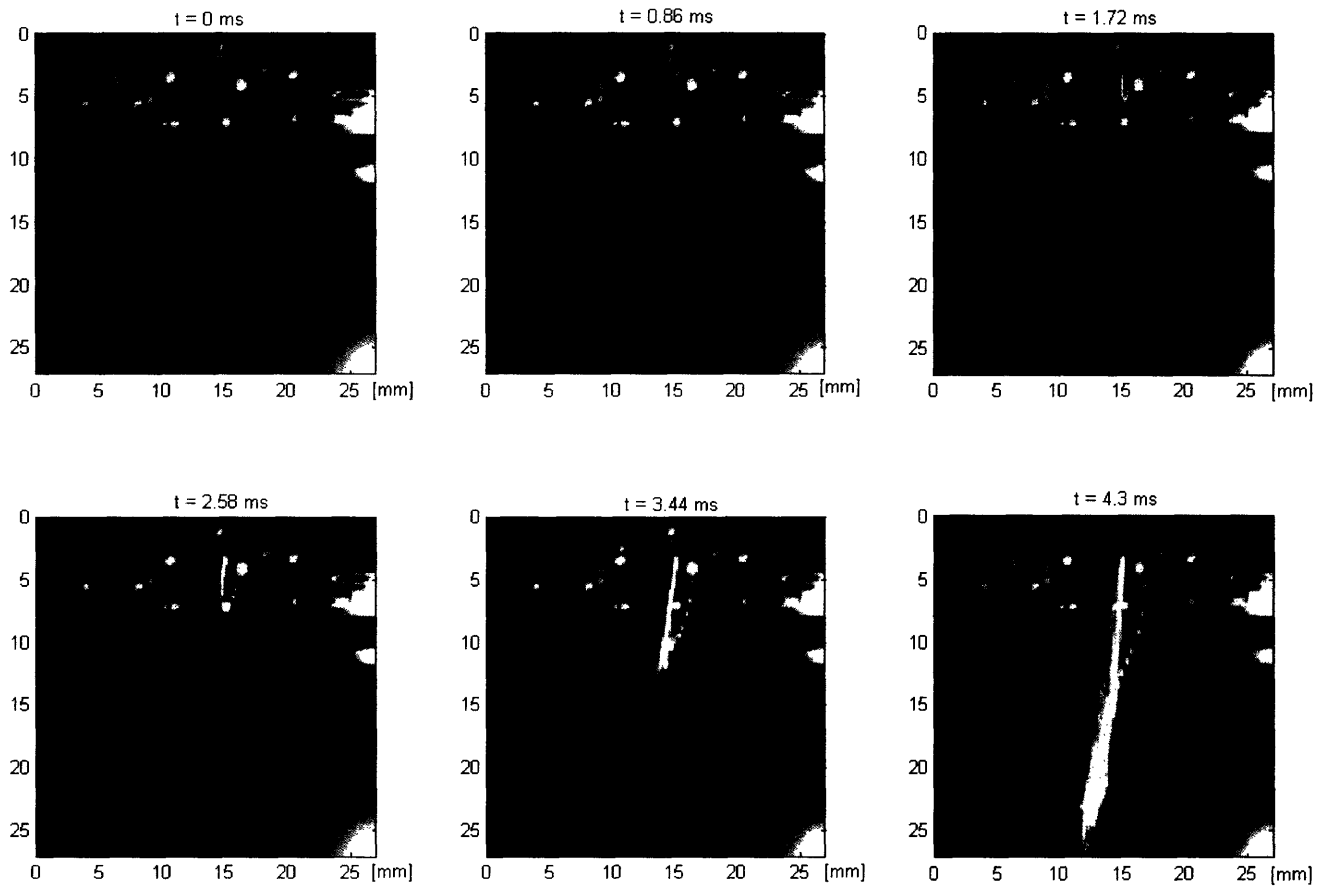

Figure 22: Water jet ejected from new nozzle design.

These are frame stills of the video of the jet ejecting from the newly manufactured nozzle. These images can be compared to video clips of the previous orifice nozzle, shown in Figure (23) below.
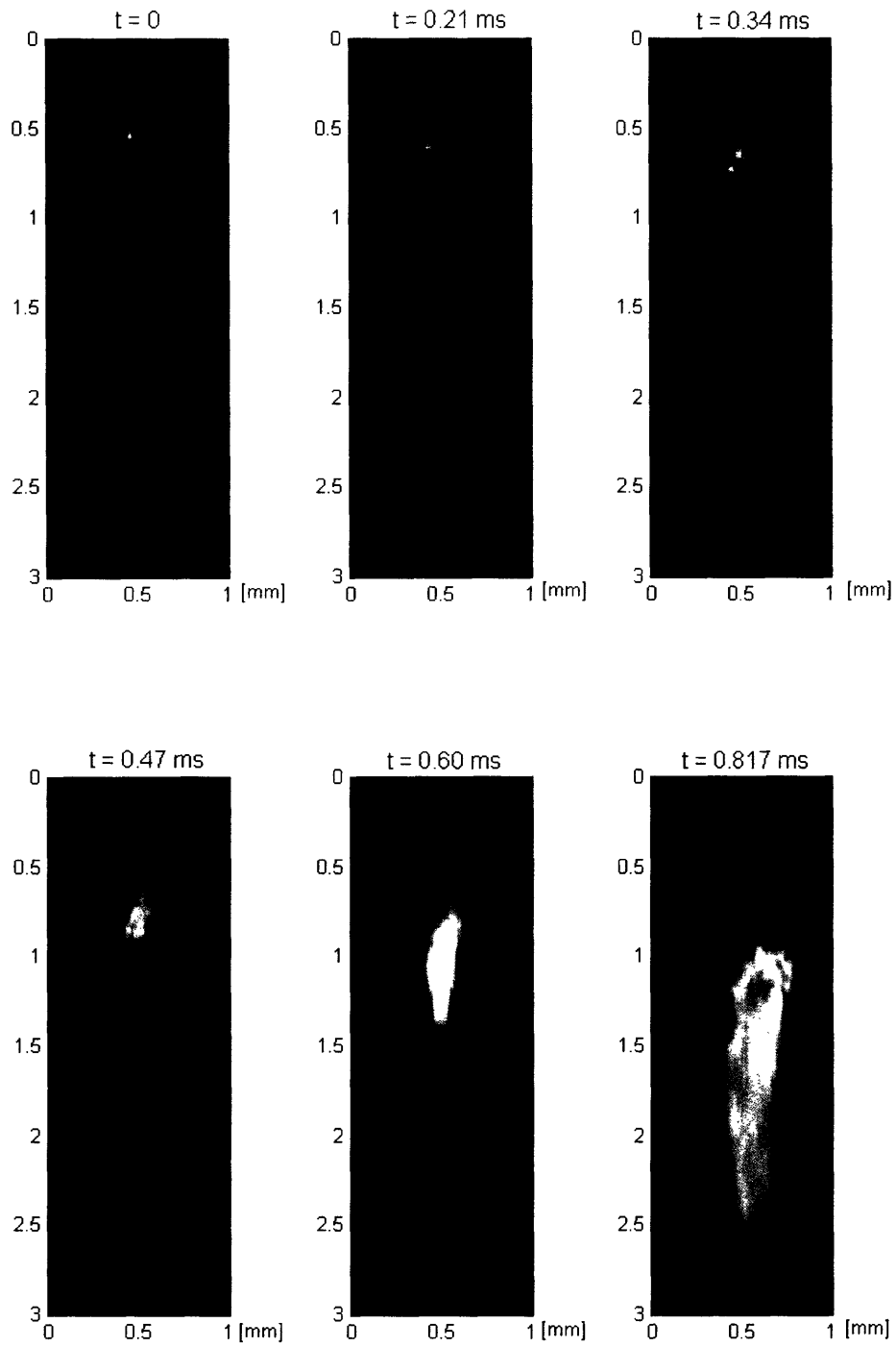
Figure 23: Water jet ejected from previous orifice nozzle.

The digital data was then analyzed by Andrea Bruno of the Bio-Instrumentation lab who produced a time plot of the jet's velocity by measuring the ratio of the flow front displacement to the frame rate interval of the camera. These time plots of jet velocity can be seen in Figures (24) and (25) below where Figure (24) represents the time dependent velocity of the new nozzle design and Figure (25) represents the time dependent velocity of the old nozzle design.

Figure 24: Velocity of the water jet leaving the new nozzle

Figure 25: Velocity of the water jet leaving the orifice nozzle.

5.0 Discussion of Results

Overall the collected data from both the finite element analysis and the experimental apparatus have shown that the new nozzle design is superior to the previous nozzle design. In the following sections the various results will be discussed in further detail.
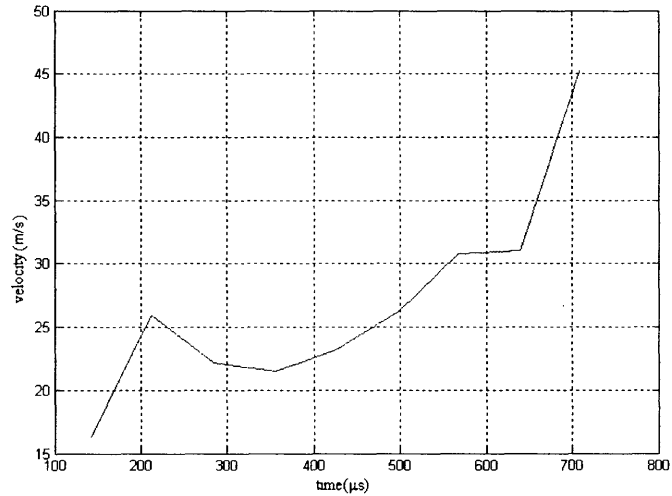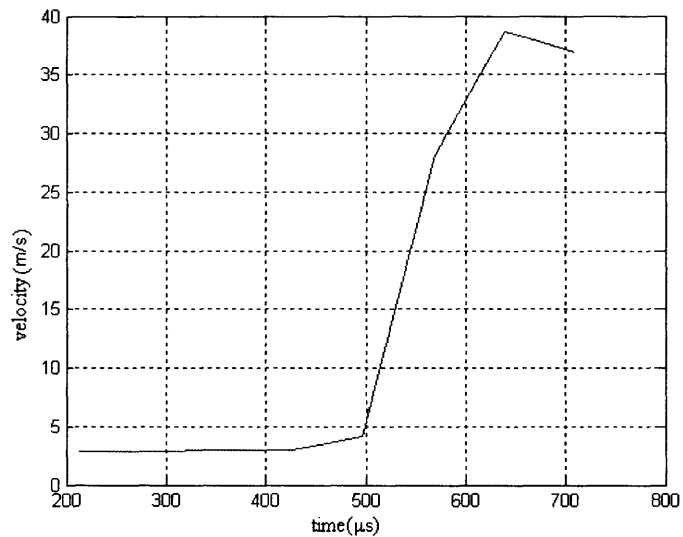
5.1 Discussion of ANSYS Results

The ANSYS results described in Section 4.1.1 appear valid. The program predicts that the discharge coefficient of the nozzle, regardless of nozzle profile, will decrease steadily with increased nozzle length. What is interesting, however, is that the different profile shapes have different dependencies on the nozzle length. As Figure(20) indicates, the linear profile is relatively unaffected by the nozzle length until it reaches a critical length of around 5mm at which point its performance drops dramatically. On the other hand, the parabolic, hyperbolic, and arc profiles show virtually similar dependencies. The performance of these nozzles drops off steeply around 4mm then begins to level off. The overall message still suggests that the shorter the nozzle transition, the better the performance of the nozzle.

The data also suggests that some profiles simply perform better than others. The previously used orifice nozzle had a predicted C_d of 0.70. If these results could be trusted, this implies that using a new nozzle of length ~ 2 mm would increase the jet velocity by almost 40 percent of its original value. Interestingly the parabolic and hyperbolic profiles performed virtually identically to each other over the complete span of nozzle lengths, and relatively similarly to the arc profile. On the other hand, the linear profile had a C_d of 0.901 for a length of 2 mm. The "arc tangent to a line" profile had a C_d of 0.957 for the same nozzle length. The "arc tangent to a line" profile also had a seemingly lower dependence on the nozzle length as indicated in Figure (20). For these reasons, the "arc tangent to a line" profile was chosen as the shape to implement in the prototype nozzle.

The verification tests performed in ANSYS gave significant confidence that the predicted results would be close to experimentally measured ones. Upon comparison, it is clear that the ANSYS curve in Figure (21) does have the proper curved shape, although it does not change as significantly with Re_d as the experimental data suggests it should. However, since ANSYS accurately modeled a long-radius nozzle, it is likely that it has done the same for the nozzles described in this thesis. It also appears that ANSYS is tending to predict values of the discharge

30

coefficient which are consistently higher than the experimentally determined values. The largest difference between these two curves occurs at a Reynolds number of approximately 10,000. At this point ANSYS predicts a C_d value of 0.97. This differs from the experimentally determined value of 0.93 by a percent error of 4.2%. Since the Reynolds number for the water jet exiting the nozzle is indeed around 10,000, this suggests that the measured performance for the injector nozzles will be close to, but lower than the predicted values by a factor of around 5%.

5.2 Discussion of Measured Results

The data collected with the injection apparatus indicates that the new nozzle is superior, although the data is somewhat sporadic. The quality of the images from the high speed camera is too low to determine whether or not the new nozzle produces a much narrower jet. In addition, there was significant variation from test to test. The velocity of the stream shown in Figure (22) was only 25 m/s at a time of 4500 µs compared 38.1 m/s at only 620 µs produced by the old orifice nozzle. When the experiment was repeated, the speed increased significantly to 45.5 m/s at 710 µs but the flow also appeared more turbulent. It is not clear what the difference was between the two tests, although they were performed on separate occasions. In any case, this demonstrated a 19% increase in velocity by the end of the injection cycle. It is important to note that the plots can not be compared point to point as the start of the data aquisition was different in each case. However the end velocities can be compared since they were measured at the end of the injection cycle.

Another problem that occurred during the testing was the fact that the nozzle did not spray directly down. For some reason the nozzle flow was skewed by an angle of 7 degrees from the axis of the nozzle. This made measuring the actual velocity of the jet leaving the nozzle difficult. In an attempt to rectify the situation, both the x and y component of the jet were calculated based on the video clip. The magnitude of the overall velocity was calculated for each data point and the curve shown in Figure (24) was created. However this still leaves the possibility that the velocity was underestimated since there is no guarantee that the water jet was traveling in the plane of the camera's focus. In addition, the video quality of both jets was too poor to make a judgment on either the shape or width of the water jet.

6.0 Conclusions

The data represented in this thesis indicate that pursuing the implementation of the new nozzle design is desirable. The increased velocity for the same energy requirement from the injection device implies that the new nozzle will be more efficient and lead to longer life of the final product. Also the increased velocity will improve the penetration of the drug and lead to more effective injections [6].

At the same time there are not enough data to conclusively determine how much better the current nozzle is. It is unclear why the test apparatus can produce such variation from test to test as seen in the new nozzle. In the future, the pressure profile measured by the apparatus will be compared to the velocity profile. This should indicate how well the velocity is mapped to the changes in pressure, and indicate the starting point of the nozzle ejection. In addition, the poor image quality of the high speed camera makes it difficult to determine accurately the velocity of the fluid front. The lighting seems insufficient for the speeds at which the jet is leaving the nozzle. Further effort in developing an adequate lighting method would be favorable. Perhaps an easier method of measuring performance would be to measure the depth of penetration into gel. Because depth of penetration is dependent on the jet velocity, this would still give an indication of how well the nozzle performed, and it is easier to measure.

The issue of the angled spray must also be addressed in future nozzle design. Not only is it difficult to measure velocity, but the jet would perform best if it shot straight down. The tilt may be a consequence of machining the wafer unevenly. One possibility is to purchase delrin sheets that are 2mm thick and cut the wafers out with a CO_2 laser cutter. This would provide a very smooth surface to drill into and may solve the problem, while providing a possibility of increased production rate.

Finally more nozzles will be created of various profiles and lengths. It may be the case that a longer nozzle will produce a more controlled jet due to the more gradual constriction of the flow. If this is the case, it may be beneficial to sacrifice some of the velocity for a more narrow and straight jet.

References

1. White, F.M. Fluid Mechanics. 5th ed., New York: McGraw-Hill. Inc, 2003, pp415-422

2. ANSYS [Web Site]. http://www.ansys.com/. 2004

3. SOLID EDGE [Web Site]. http://www.solid-edge.com/. 2004

4. Mitragotri, Samir and Joy Schramm-Baxter. "Needle-free jet injections: dependence of
   jet penetration and dispersion in the skin on jet power." *Science Direct*. 10 April
   2004 [Web Site] http://www.sciencedirect.com

5. Incopera, F. and D. DeWitt. Fundamentals of Heat and Mass Transfer 5th ed., New York: John
   Wiley & Sons. Inc, 2002, pp466-471

6. Mitragotri, S. and Schramm-Baxter, J. Transdermal Drug Delivery by Jet Injectors: Energetics
   of Jet Formation and Penetration. *Science Direct*. 25 July 2002
   [Web Site] http://www.sciencedirect.com

7. Mitragotri, S. and Schramm-Baxter, J and Katrencik, J. Jet injection into polyacrylamide gels:
   investigation of jet injection mechanics. *Science Direct*. 8 December
   2003 [Web Site] http://www.sciencedirect.com

Appendix A

Results from ANSYS simulations.

Nozzle Profile	Applied Pressure(Mpa)	Nozzle Length(mm)	Average Ve(m/s)	Vb(m/s)	Cd
orrifice (current nozzle)	5	10 (fixed length)	70	100	70
linear	5	2	90.1	100	0.901
		4	89.9	100	0.899
		6	84.5	100	0.845
		8	59	100	0.59
parabolic	5	2	93.4	100	0.934
		4	79.4	100	0.794
		6	51.5	100	0.515
		8	43.3	100	0.433
hyperbolic	5	2	93.35	100	0.9335
		4	79.409	100	0.79409
		6	51.537	100	0.51537
		8	43.278	100	0.43278
arc	5	2	92.5	100	0.925
		4	83.1	100	0.831
		6	51	100	0.51
		8	43.5	100	0.435
arc+l	5	2	95.7	100	0.957
		4	92.5	100	0.925
		6	87.2	100	0.872
		8	80.9	100	0.809

Table of Discharge coefficients determined by ANSYS for various nozzles.